Optical properties of breast tumor phantoms containing carbon nanotubes and nanohorns

Saugata Sarkar
Abhijit A. Gurjarpadhye
Christopher G. Rylander
Marissa Nichole Rylander

SPIE

Optical properties of breast tumor phantoms containing carbon nanotubes and nanohorns

Saugata Sarkar,[a] **Abhijit A. Gurjarpadhye,**[b] **Christopher G. Rylander,**[a,b] **and Marissa Nichole Rylander**[a,b]
[a]Virginia Tech, Department of Mechanical Engineering, ICTAS Building, Stanger Street, Blacksburg, Virginia 24061
[b]Virginia Tech and Wake Forest University, School of Biomedical Engineering and Sciences, Blacksburg, Virginia 24061

Abstract. The degree by which optical properties of tumors are altered following introduction of carbon nanotubes (CNTs) of varying concentration and type is poorly understood, making it difficult to predict the impact of CNT inclusion on the photothermal response to laser therapies. Optical properties were measured of phantoms representative of breast tumor tissue incorporated with multiwalled carbon nanotubes (MWNTs), single-walled carbon nanotubes (SWNTs), and single-walled carbon nanohorns (SWNHs) of varying concentration (0.01–0.1 mg/ml). Tissue phantoms were made from sodium alginate (3 g/ml) incorporated with polystyrene microbeads (3 μm diam and 1 mg/ml) and talc-France powder (40 mg/ml). Absorption (μ_a) and reduced scattering (μ_s') coefficients of phantoms containing CNTs were determined by the inverse adding-doubling algorithm for the wavelength range of 400–1300 nm. Optical properties of phantoms without CNTs were in the range of $\mu_a = 1.04$–0.06 mm^{-1} and $\mu_s' = 0.05$–0.07 mm^{-1} at a wavelength of 900 nm, which corresponds with published data for human breast tumor tissue. Incorporating MWNTs, SWNTs, and SWNHs in phantoms with a concentration of 0.1 mg/ml increased (μ_a) by 20- to 30-fold, 5- to 6-fold, and 9- to 14-fold, respectively, for the wavelength range of 800–1100 nm with minimal change in μ_s' (1.2- to 1.3-fold). Introduction of CNTs into tissue phantoms increased absorption, providing a means to enhance photothermal therapy. © *2011 Society of Photo-Optical Instrumentation Engineers (SPIE).* [DOI: 10.1117/1.3574762]

Keywords: cancer therapy; nanoparticles; laser treatments; oncology; soft tissue composites.

Paper 10594SSR received Nov. 4, 2010; revised manuscript received Feb. 21, 2011; accepted for publication Feb. 28, 2011; published online May 20, 2011.

1 Introduction

Inclusion of light-absorbing nanoparticles into tumors undergoing laser therapy can increase the absorption coefficient and thus photothermal generation within the targeted tissue volume. Laser therapies with nanoparticle inclusion can potentially achieve a greater efficacy, treat larger tumor volumes, and require shorter treatment durations due to the increased heat deposition and thermal diffusion in the tumor.[1–7] Carbon nanotubes (CNTs) have received attention for their potential role as thermal enhancers for laser ablation and drug delivery.[8,9] CNTs are composed of graphene sheets with sp^2-bonded carbon atoms rolled seamlessly into a tubular form. The two major types of CNTs are single-walled nanotubes (SWNTs), which have one seamless tube, and multiwalled nanotubes (MWNTs), which possess two or more concentric tubes. The diameter and length of SWNTs are 1.5–3.0 and 20–1200 nm, respectively, whereas the corresponding diameter and length dimensions for MWNTs are 5.0–100 nm and 1–50 μm, respectively.[3,10–14] Another unique embodiment of SWNTs is the single-walled carbon nanohorn (SWNH), which is composed of an aggregate of cone-shaped SWNTs with individual diameters of 1–1.5 nm. The spiny agglomerate SWNH structure has an overall diameter of 50–100 nm.[15,16] CNTs possess exceptional electromagnetic, thermal, and chemical properties. A remarkable property of CNTs (both metallic and semiconducting) is their ability to absorb electromagnetic energy in the near-infrared optical tissue window (700–1100 nm) leading to volumetric heat generation at clinically relevant tissue depths.[1,3,17] Light within this optical window has been shown to penetrate human skin with 1/e penetration depths of 1.6–2 mm.[18] The length of a CNT has considerable impact on its ability to absorb light. Efficient light absorption occurs when the length of the CNT is at least half the wavelength of the incident light. Based on antenna theory,[19–22] CNT lengths of 900–1200 nm have been shown previously by our group to possess significant light absorption at a wavelength of 1064 nm, leading to heat generation capable of tumor destruction.[1–3,23,24] However, limited information exists regarding the optical properties (absorption and scattering coefficients) of solutions or tissues containing CNTs of varying type and concentration. This information is critical for appropriate selection of CNTs for designing therapies utilizing laser treatment and nanoparticles.

Previous studies have measured a variety of optical properties, including refractive index, absorbance, transmittance, reflectance, and scattering coefficients of CNTs in liquid solutions.[8,25–35] Jeong et al. measured attenuation and extinction coefficients of SWNTs in water by optical absorption spectroscopy in the wavelength range of 270–1000 nm.[33] Khudyakov et al. measured the optical absorption coefficient of SWNTs in carboxymethyl cellulose thin polymer film by the Z-scan method and found absorption coefficients to be nonlinear with different pulsed laser intensities (20–50 MW/cm^2).[35] Aside from these initial studies, this will be the first paper comparing the absorption and scattering properties of SWNTs, MWNTs, and

Address all correspondence to: Marissa Nichole Rylander, Virginia Tech, Department of Mechanical Engineering and School of Biomedical Engineering and Sciences, Nanotherapeutics and Bioheat Transfer Lab, ICTAS Building, Stanger Street, RM335, Blacksburg, VA, 24061. Tel: 540-231-3134; E-mail: mnr@vt.edu.

SWNHs in water and in tissue representative phantoms for identical wavelengths and concentrations of CNTs.

Different computational techniques can be used to compute absorption and reduced scattering coefficients, such as Kubelka–Munk approach,[36] inverse Monte Carlo method,[37–39] and inverse adding-doubling (IAD) method.[40] We chose to use the IAD method to determine the optical properties of water and phantoms containing CNTs due to its accuracy and rapid computing time. IAD requires transmittance, reflectance, and refractive index as input parameters in order to calculate absorption and reduced scattering coefficients. Others have used inverse and forward adding doubling to obtain the optical properties of tissue and phantoms.[40–42] However, prior studies have not determined the absorption and reduced scattering coefficient of tissues or representative tissue phantoms incorporated with CNTs.

In this paper, we determined the attenuation, absorption, and scattering coefficients of two different media: (*i*) water and (*ii*) representative breast tumor phantoms with optical properties identical to breast tissue, both containing CNTs of varying types (SWNTs, MWNTs, and SWNHs) and concentrations (0.01–0.1 mg/ml). The difference in interfacial effects between CNTs and the corresponding liquid or solid phantoms may affect the optical properties of the samples; therefore, optical properties were measured for CNTs in both types of media. Knowledge of the effect of varying CNT type and concentration on solutions and breast tumor tissue optical properties will enable selection of the appropriate CNT type and concentration for a desired level of photothermal generation in the tissue and permit prediction of tissue response to nanoparticle-enhanced laser therapies.

2 Materials and Methods

2.1 *Water-Soluble Carbon Nanotubes*

MWNTs were synthesized by Dr. David Carroll's group at Wake Forest University,[1,3] SWNTs were purchased from SES Research Inc. (Texas) and SWNHs were synthesized by Dr. David Geohegan's group at Oak Ridge National Laboratories.[43,44] The lengths of MWNTs and SWNTs ranged from 900–1200 nm. Outer diameters of the MWNTs were in the range of 40–60 nm, whereas SWNT outer diameters were <2 nm. Individual SWNHs had diameters of 1–1.5 nm with agglomeration lengths of 50–100 nm. The purity of all CNTs was confirmed to be >95% by thermogravimetric analysis, dynamic light scattering, and transmission electron microscopy (data not included).[45]

MWNTs, SWNTs, and SWNHs are naturally hydrophobic and not soluble in polar solvents, such as water. All types of CNTs were made water soluble by functionalizing their outer surfaces with 1% w/v concentration of Pluronic F-127 purchased from Biotium, Inc. Pluronic at this concentration has been shown to provide desired CNT solubility and is nontoxic *in vitro* and *in vivo*.[1,23] CNTs in the pluronic-water solutions were sonicated for 40–50 min to make desired concentrations for measurement of optical properties of water solutions containing CNTs.

2.2 *Tissue Phantom Preparation*

Tissue representative phantoms were created with optical properties similar to that of breast tumor tissue. Tissue representative phantoms were produced from sodium alginate Protanal LF
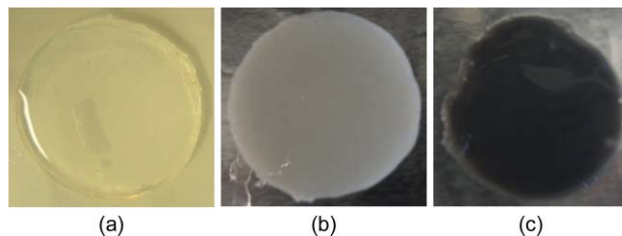

Fig. 1 (a) Sodium alginate phantom, (b) phantom with inclusion of polystyrene beads and talc powder, and (c) phantom with polystyrene beads, talc powder, and CNTs.

10/60 (FMC Biopolymer, Drammen, Norway), a low-viscosity alginate with a mean guluronate/mannuronate ratio of 70% and mean molecular weight of 180 kDa. Sodium alginate is transparent and does not adequately reflect the intrinsic scattering properties of biological tissues. In order to create phantoms that possess optical properties representative of breast tumor tissue, light scattering and absorbing polystyrene beads and highly light scattering talc-France perfume powder were evenly mixed with sodium alginate.[46,47] The final formulation utilized to achieve the optical properties of breast tumor tissue was talc-France perfume powder (40 mg/ml concentration) and polystyrene beads (3 μm diam, 1 mg/ml concentration) in sodium alginate aqueous gel.

Next, the CNT phantom composite tissue structures were created. Three concentrations (0.01, 0.05, and 0.1 mg/ml) of CNTs were suspended in 1% pluronic water. The concentration range was selected based on prior studies showing 0.01–0.1 mg/ml caused minimal toxicity while enabling significant heat generation.[1,3,17,23] Sodium alginate was stirred vigorously with pluronic water containing CNTs, polystyrene beads, and talc powder to a 3% w/v concentration for 1 h. The final solution was cross-linked with calcium chloride for 1 h.[48,49] All samples were approximately 800 μm thickness to permit adequate light transmission necessary for spectrophotometric measurement[50] [Figs. 1(a)–1(c)]. The radius (35 mm) of the cylindrical samples was made large enough to completely cover the reflection and transmission ports of the integrating sphere accessory of the spectrophotometer. For each concentration and type of CNT, five experimental samples ($N = 5$) were made and all results were represented as the mean values of these samples.

2.3 *Spectrophotometry*

A Cary 5000 Spectrophotometer (Varian Inc., North Carolina) was used to measure transmittance, reflectance, and absorbance of liquid and phantoms with and without CNTs in the wavelength range of 300–1300 nm. A diffuse reflectance accessory (DRA 2500) was mounted in the spectrophotometer to allow measurement of diffuse scattering effects. Ballistic-light intensity was measured for 100% transmission (in the absence of sample, I_{0T}) and 100% reflection (using a reflectance standard, I_{0R}) to obtain baseline values. Sample transmittance, reflectance, and absorbance were calculated based on measured light intensity, I_s, at the detector, depending on position of the sample in the DRA [Figs. 2(a)–2(e)].

When samples were mounted at the transmission and reflection ports of the integrating sphere, transmittance (*T*) and
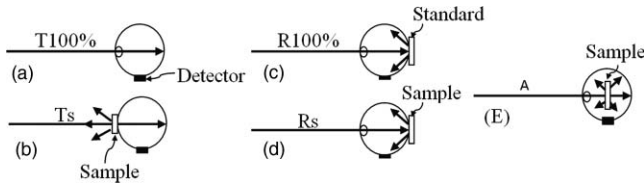
Fig. 2 Sample position in the DRA in order to measure transmittance, reflectance, and absorbance. Sample position for (a) 100% transmittance and (b) actual sample transmittance. Sample position for measuring (c) 100% reflectance and (d) actual sample reflectance. Sample position for (e) measuring absorbance.

reflectance (R) are expressed as $T = I_{sT}/I_{0T}$ and $R = I_{sR}/I_{0R}$, respectively. Light attenuation in a sample follows the Beer–Lambert law relationship and is expressed in Eq. (1). The total attenuation coefficient (μ_t) is the summation of absorption (μ_a) and scattering coefficient (μ_s), expressed in Eqs. (2) and (3),

$$\frac{I_s}{I_0} = e^{-\mu_t d}, \tag{1}$$

$$\mu_t = \mu_a + \mu_s, \tag{2}$$

$$\mu_t = -\frac{1}{d} \ln T, \tag{3}$$

where d is sample thickness and T is transmittance.

In order to determine absorption coefficients (μ_a), CNT solutions were placed in the center of the integrating sphere allowing the spectrophotometer to detect the intensity of light not absorbed by the sample [Fig. 2(e)]. The absorption coefficient is expressed as follows:

$$\mu_a = -\frac{2.303}{d} \ln \frac{I_s}{I_0}. \tag{4}$$

Equations (3) and (4) were used to determine attenuation and absorption coefficients for water containing CNTs. The center mount technique was not suitable for measuring optical properties of tissue phantoms due to their geometry (d is not consistent in all directions). Rather diffuse transmittance and reflectance measured by the spectrophotometer served as input parameters to the IAD method, allowing determination of the absorption and reduced scattering coefficients.

2.4 Inverse Adding-Doubling Method

The IAD technique was used to calculate the absorption and reduced scattering coefficients for breast cancer phantoms with CNT inclusion. Assumptions can be made such that a soft turbid tissue behaves as an isotropic media and only diffuse transmittance and reflectance are required to measure absorption and reduced scattering coefficients.[50] According to this assumption, scattering can be expressed in terms of reduced scattering coefficient, $\mu_s' = \mu_s(1 - g)$, where μ_s is the scattering coefficient and g is the anisotropy factor. The IAD method determined optical properties by inverse calculation of the radiative transport equation,[50] where samples require homogenous optical properties with infinite plane parallel slabs. During computation, this method assumed a set of initial values of albedo (a'), optical thickness (b'), and sample thickness (δ),[40,50] which are expressed in Eqs. (5) and (6). These optical properties are expressed in terms of absorption and reduced scattering coefficients in Eqs. (7) and (8). Absorption (μ_a) and reduced scat-

tering (μ_s') coefficients are calculated from albedo and optical thickness in Eqs. (7) and (8). The IAD method calculates transmittance and reflectance based on assumed values of optical properties and compares the values of R and T with the corresponding experimentally measured parameters. If the values are not identical, then it assumes a new set of values for optical parameters. The process continues until the calculated reflectance and transmittance values are identical to the experimental values, yielding the most accurate values of optical properties,

$$a' = \frac{\mu_s'}{\mu_s' + \mu_a}, \tag{5}$$

$$b' = \delta(\mu_s' + \mu_a), \tag{6}$$

$$\mu_a = \frac{(1 - a')b'}{\delta}, \tag{7}$$

$$\mu_s' = \frac{a'b'}{\delta}. \tag{8}$$

2.5 Optical Coherence Tomography

Optical coherence tomography (OCT) is a ballistic optical imaging technique.[51,52] OCT was employed in this study to measure refractive index of phantoms, according to the technique of Sorin and Grey.[53] Refractive index was a necessary input parameter to the IAD algorithm. When an optically transparent sample is placed in the incident beam, light is reflected from both the first incident plane (air-to-solid interface) and the second incident plane (solid-to-air interface) of the sample due to the mismatch of refractive index. The optical thickness (OPL) of the sample can be represented as the distance between two reflection peaks of two incident planes. Physical thickness (d) of a sample is represented as the difference between OPL of the sample and optical displacement of a stationary mirror before and after placing the sample in the incident beam. Refractive index is determined by the ratio between optical thickness to the physical thickness (d) of the sample ($n_g = $ OPL/d).

2.6 Experimental and Computational Validation

In order to validate our experimental measurement technique and IAD algorithm, we determined the optical properties of pig skin and compared our results to previously reported values by Beek et al.[54] Fresh pig skin was collected immediately after animal sacrifice with subsequent removal of hair and subcutaneous fat. The optical properties of five samples with a thickness of 1 mm were measured.

3 Results

3.1 Total Attenuation and Absorption Coefficients of Carbon Nanotubes in Water

The total attenuation coefficients of MWNTs, SWNTs, and SWNHs of varying concentration (0.01–0.1 mg/ml) in water for the wavelength range of 300–1300 nm are shown in Figs. 3(a)–3(c). Inclusion of any of the three CNTs in water
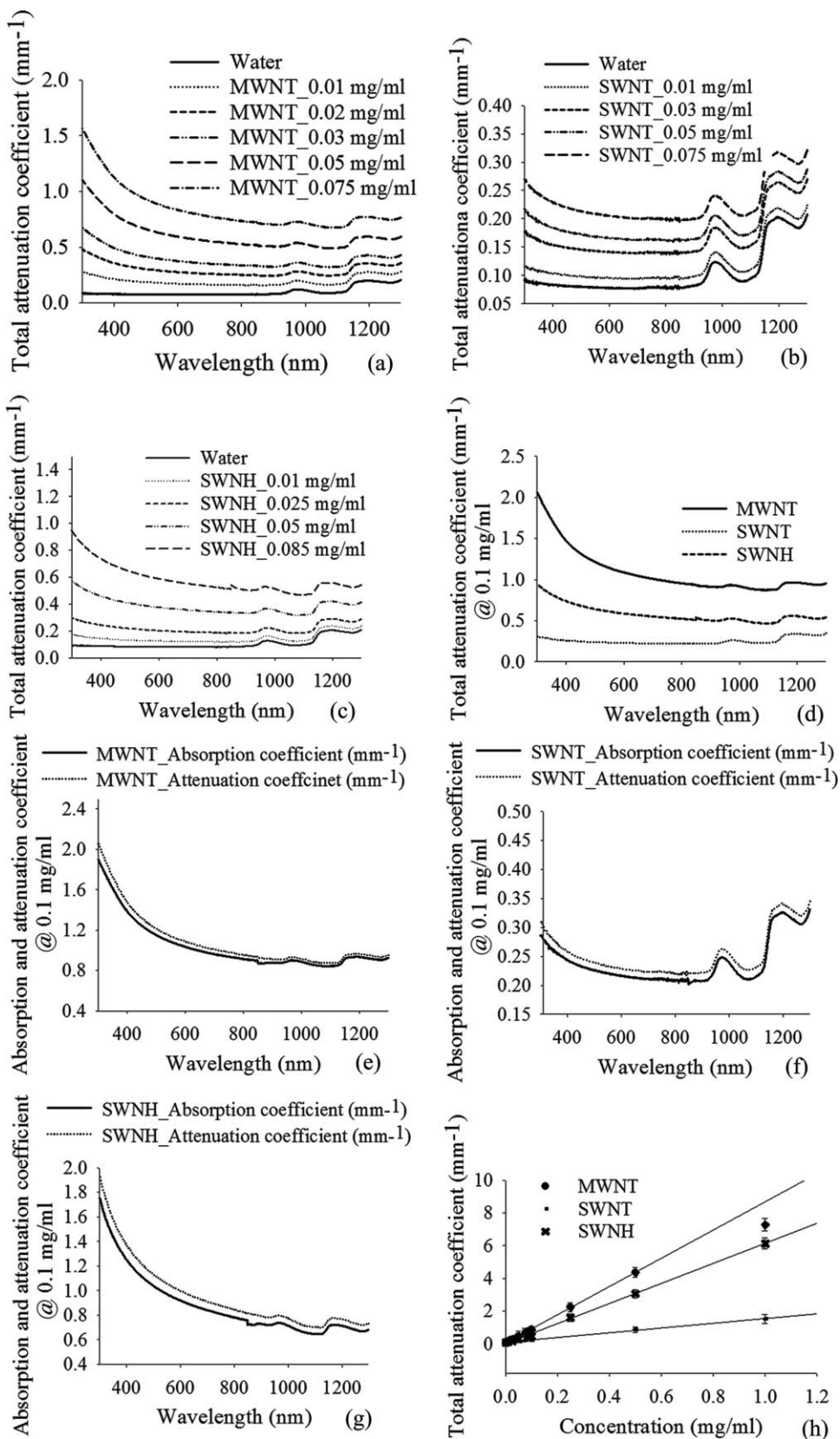
Fig. 3 Total attenuation coefficients (in millimeters^{-1}) of (a) MWNTs, (b) SWNTs, and (c) SWNHs in water for varying concentration (0.01–0.1 mg/ml), (d) attenuation coefficients of MWNTs, SWNHs, and SWNTs in water compared for a concentration of 0.1 mg/ml, absorption and attenuation coefficient of (e) MWNTs, (f) SWNTs, and (g) SWNHs for a CNT concentration of 0.1 mg/ml, and (h) total attenuation coefficient of all three types of CNTs as a function of concentration.

caused a significant increase in attenuation across all wavelengths compared to water. The total attenuation coefficient of any of the three CNT solutions increases with higher CNT concentration. The attenuation coefficients of all three CNT types were compared at a concentration of 0.1 mg/ml, as shown in Fig. 3(d). Water-containing MWNTs possess the greatest level of attenuation compared to water containing SWNTs and SWNHs. Attenuation coefficients of MWNTs in water are approximately four times higher than SWNTs and two times higher than SWNHs at a concentration of 0.1 mg/ml and wavelength of 1064 nm.

Total attenuation and absorption coefficients of CNTs were measured and compared for a concentration of 0.1 mg/ml in Figs. 3(e)–3(g). The comparisons were made to determine the contribution of CNTs to optical scattering and absorption. Total attenuation coefficients were approximately 1.03–1.08 times higher than absorption coefficients for the same range of wavelengths (300–1300 nm) for the above-mentioned CNTs. The curves representing the attenuation and absorption coefficients are nearly identical, implying the contribution of scattering to attenuation is <8%, when CNTs are evenly dispersed in media. The attenuation coefficients of CNTs in water were compared at a wavelength of 1064 nm for varying CNT concentration (0–1.0 mg/ml) and were observed to be linearly correlated with concentration [Fig. 3(h)], which satisfies Beer's law. Higher CNT concentration produces increased attenuation. However, the linear relationship of attenuation coefficient with MWNT concentration becomes nonlinear for concentrations of 0.5 mg/ml or greater. All results are the mean of five

experimental measurements ($N = 5$) with an average standard deviation of ± 0.03–0.08 for the wavelength range of 300–1300 nm.

3.2 Optical Properties of Tissue Phantoms

Diffuse transmittance and reflectance of sodium alginate phantoms incorporated with polystyrene beads (3 μm diam and 1.0-mg/ml concentration) and talc perfume powder (0–40 mg/ml) were measured with a spectrophotometer. Figure 4(a) shows the values of diffuse transmittance and reflectance in the wavelength range of 300–1300 nm for phantoms when 1.0 mg/ml polystyrene beads and 40 mg/ml of talc perfume powder were added. The measured transmittance and reflectance were used as inputs to the IAD algorithm and permitted determination of the corresponding absorption and reduced scattering coefficients shown in Figs. 4(b) and 4(c).

Without incorporating polystyrene beads and talc, the absorption coefficients of sodium alginate phantoms (97% water) were found to have a similar absorption spectra and peaks as water at 970 and 1200 nm [Fig. 4(b)][50,55] and scattering was found to be negligible [Fig. 4(c)]. After incorporating polystyrene beads (1.0 mg/ml) in phantoms, both absorption and scattering increased. Inclusion of polystyrene beads alone caused the phantom to possess an absorption coefficient similar to breast cancer tissue; however, the reduced scattering coefficient was not sufficient to mimic actual breast cancer tissue. In order to increase the reduced scattering coefficient for the phantoms, talc powder with concentrations of 0–40 mg/ml was introduced in the phantom in
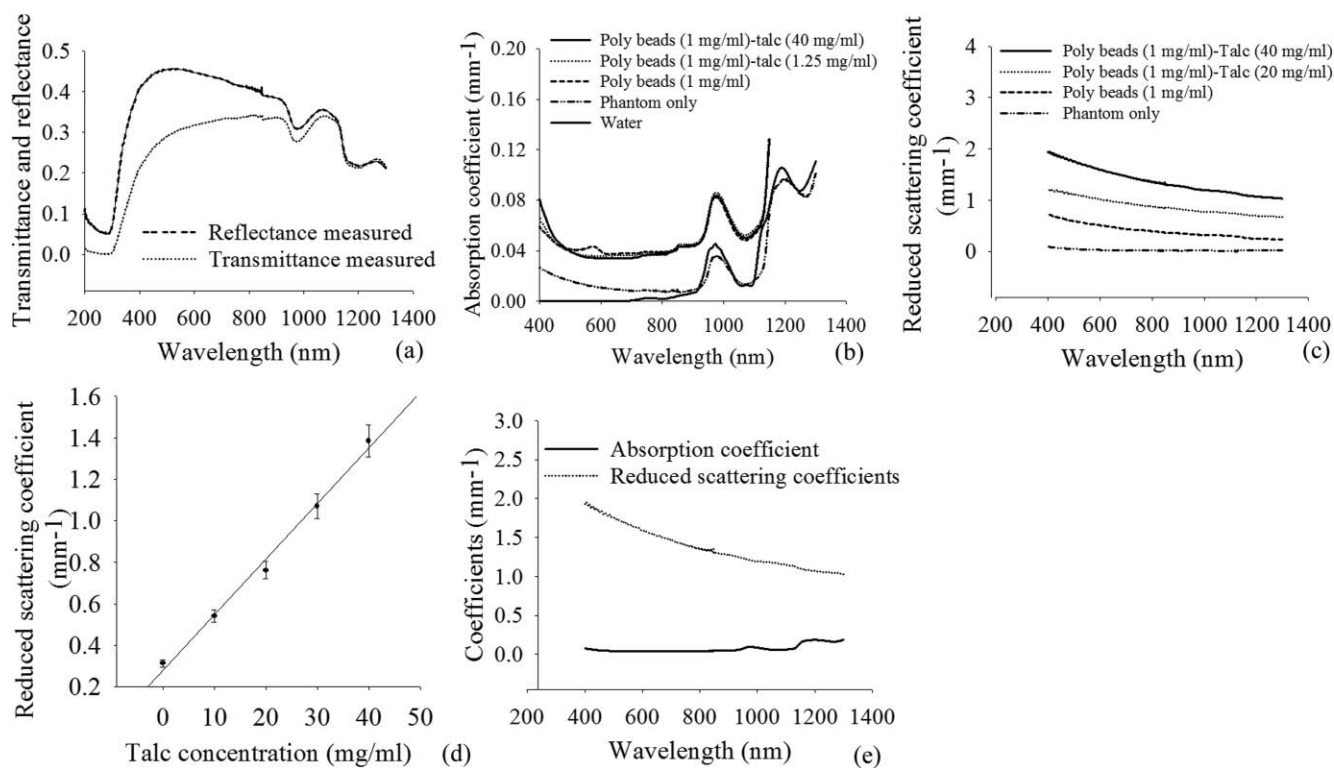

Fig. 4 (a)Transmittance and reflectance of phantoms incorporated with talc powder (1 mg/ml) and polystyrene beads (40 mg/ml) measured with a spectrophotometer and computed by IAD. (b,c) Absorption and reduced scattering coefficients of phantoms with varying concentration of polystyrene beads (0 and 1.0 mg/ml) and talc powder (0–40 mg/ml). (d) Reduced scattering coefficient as a function of talc powder concentrations. (e) Absorption and reduced scattering coefficients of sodium alginate phantoms with polystyrene beads (1 mg/ml) and talc (40 mg/ml) computed by the IAD method.

Table 1 Optical properties of actual breast cancer tissue and breast cancer phantom.

Wavelength (nm)	Reduced scattering coefficient (mm^{-1})		Absorption coefficient (mm^{-1})	
	Breast tumors	Breast phantoms	Breast tumors	Breast phantoms
800	0.7–1.4	1.35–1.58	0.02–0.07	0.04–0.05
900	0.8–1.2	1.22–1.5	0.05–0.07	0.04–0.06

combination with polystyrene beads. For all concentrations of talc, absorption coefficients were unchanged [Fig. 4(b)]; however, the reduced scattering coefficient increased as a function of talc concentration [Fig. 4(c)]. The change in scattering coefficient with varying talc concentrations is represented in Fig. 4(d), where scattering is linearly related with talc concentration. The final concentration of talc (40 mg/ml) and polystyrene beads (1 mg/ml) in sodium alginate phantoms represent similar optical properties to breast cancer phantoms shown in Fig. 4(e). All experiments were conducted with five experimental samples ($N = 5$), and all results were considered as the mean of five experimental samples with standard deviation of $\pm$ 0.02–0.08 for the wavelength range of 400–1300 nm.

Absorption and reduced scattering coefficients of breast cancer phantoms were compared to previously published human breast cancer tissue[50,56,57] at 800 and 900 nm in Table 1. At a wavelength of 800 nm, absorption and reduced scattering coefficients of breast cancer phantoms ($\mu_a = 0.04$–0.05 mm^{-1} and $\mu'_s = 1.35$–1.58 mm^{-1}) were found to correspond closely with human breast cancer tissue ($\mu_a = 0.02$–0.07 mm^{-1} and $\mu'_s = 0.7$–1.4 mm^{-1}). The phantom optical properties were also found to be similar to breast tissue for a wavelength of 900 nm, where the absorption and reduced scattering coefficients of breast cancer phantom are $\mu_a = 0.04$–0.06 mm^{-1} and $\mu'_s = 1.22$–1.5 mm^{-1} and those for human breast cancer tissue are $\mu_a = 0.05$–0.07 mm^{-1} and $\mu'_s = 0.8$–1.2 mm^{-1}.

3.3 Model Validation

Prior to measuring optical properties of tissue representative phantoms and their CNT composites, optical properties of pig skin were determined in order to validate our experimental measurement technique and IAD algorithm. Figure 5 shows absorption and reduced scattering coefficients of pig skin computed by the IAD method for the wavelength range of 400–1300 nm. Our measured absorption and reduced scattering coefficients of pig skin correspond closely with the experimental results of Beek et al.[54] at wavelengths of 632.8, 790, and 850 nm, confirming the accuracy of our measurement and computational techniques.

3.4 Refractive Index

The refractive indices (n) of phantoms, in combination with polystyrene beads, talc powder, and CNTs, were measured with OCT at a wavelength of 1310 nm. The values were found to vary between 1.39 and 1.41 and used as input parameters to the IAD

model. Refractive index (1.37) of sodium alginate phantoms without polystyrene beads, talc, and CNTs was measured by Esteban et al.[58] Our measured values (refractive index) of breast cancer representative phantoms was higher than Esteban et al.,[58] due to the presence of talc (40 mg/ml) with refractive index,[59] $n = 1.586$ and polystyrene beads (1 mg/ml) with refractive index,[60] $n = 1.592$.

3.5 Breast Cancer Phantom–Carbon-Nanotube Composites

The diffuse transmittance and reflectance of breast cancer phantoms incorporated with MWNTs of varying concentration are shown in Figs. 6(a) and 6(b), respectively. Both transmittance and reflectance decreased with increasing MWNT concentration due to the significant degree of absorption by MWNTs. Absorption and reduced scattering coefficients of phantoms containing MWNTs are shown in Figs. 6(c) and 6(d). These properties were computed by IAD based on measured transmittance and reflectance shown in Figs. 6(a) and 6(b). Absorption and reduced scattering coefficients of phantoms containing SWNTs and SWNHs were computed in a similar manner and are shown in Figs. 6(e)–6(h).

For all types of CNTs, absorption coefficient increased with greater CNT concentration. Inclusion of MWNTs caused the absorption coefficients of phantoms (0.1 mg/ml) to increase by 21 times compared to phantoms without MWNTs [Fig. 6(c)] at a wavelength of 1064 nm. Absorption coefficients of phantoms containing SWNTs and SWNHs increased by five
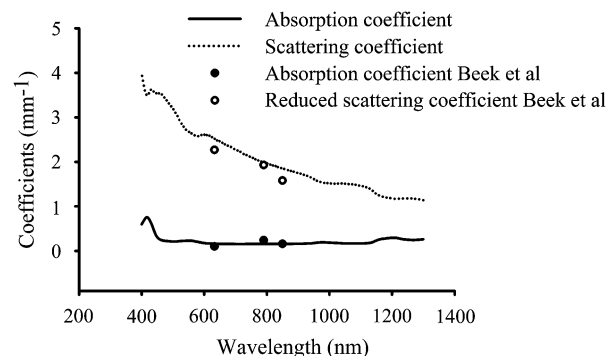
Fig. 5 Absorption and reduced scattering coefficients of pig skin measured by our group and compared to the experimental results of Beek et al. (Ref. 54).
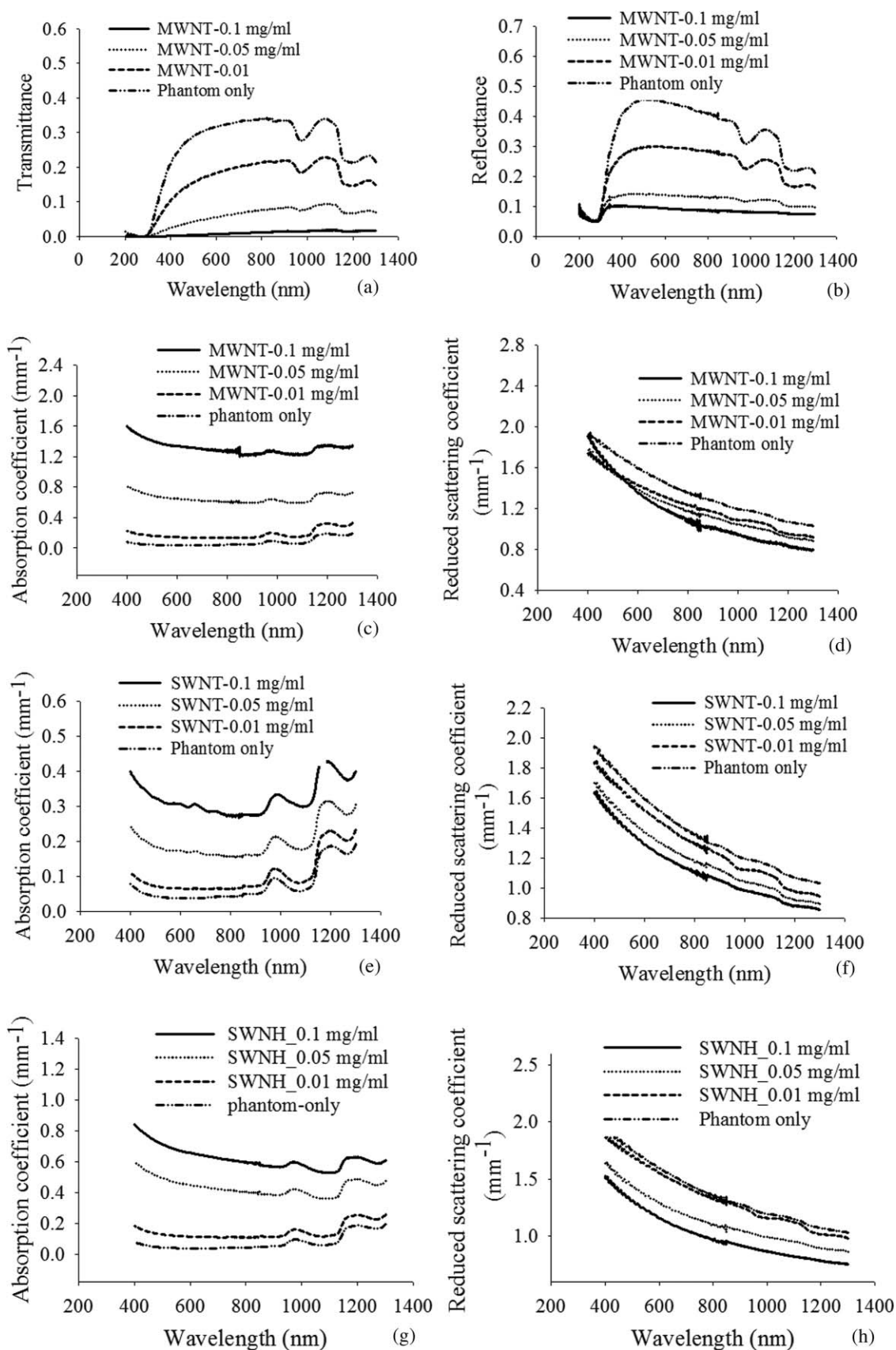
Fig. 6 (a) Measured transmittance and (b) reflectance of breast cancer phantoms containing MWNTs of varying concentration (0.01, 0.05, and 0.10 mg/ml) for the wavelength range of 400–1300 nm. Absorption coefficient and reduced scattering coefficient of breast cancer phantoms containing (c,d) MWNTs, (e,f) SWNTs, and (g,h) SWNHs of varying concentration determined with the IAD method for the wavelength range of 400–1300 nm.
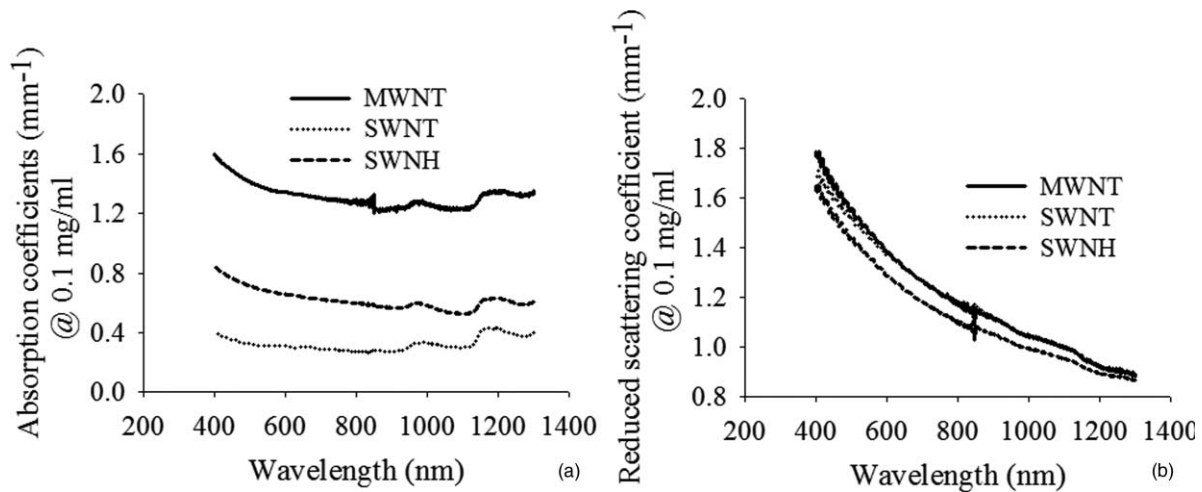
Fig. 7 (a) Absorption and (b) reduced scattering coefficients of phantoms containing MWNTs, SWNTs, and SWNHs for an identical concentration of 0.1 mg/ml.

and nine times, respectively, for the same CNT concentration (0.1 mg/ml) and wavelength (1064 nm) compared to phantoms without CNTs [Figs. 6(e) and 6(g)]. Reduced scattering coefficients of phantoms with 0.1 mg/ml CNTs increased with values of 1.2–1.3 times greater compared to phantoms without CNTs [Figs. 6(d), 6(f), and 6(h)]. Trends described for a wavelength of 1064 nm were observed for all wavelengths considered. These results suggest that CNTs are predominantly absorbing particles with little contribution to scattering.

The absorption coefficient of phantoms containing varying types of CNTs were compared for an equal concentration 0.1 mg/ml [Fig. 7(a)]. Phantoms containing MWNTs have the largest absorption coefficients. Absorption of phantoms containing MWNTs is about four times higher than phantoms containing SWNTs and approximately two times higher than phantoms containing SWNHs at the wavelength of 1064 nm. The absorption coefficient of phantoms with SWNHs is about two times higher than phantoms with SWNTs at the same wavelength. The variation in reduced scattering coefficient was at most 10% for all CNTs at the same concentration and wavelength [Fig. 7(b)].
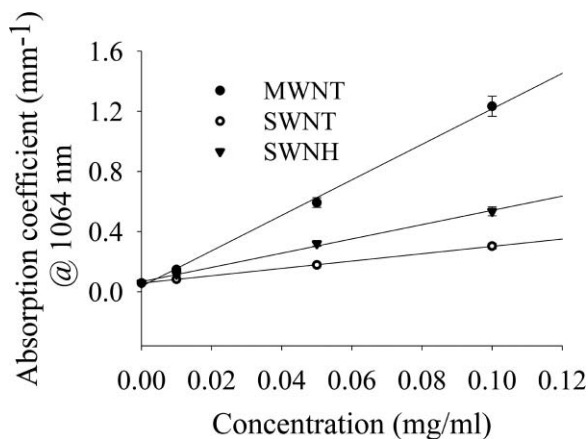
The absorption coefficients of breast cancer phantoms with CNT inclusion for a range of concentrations (0.0–0.1 mg/ml) of CNTs were found to be linearly related to concentrations (Fig. 8) at a wavelength of 1064 nm. Figure 8 can be used for determining the absorption coefficients of breast cancer tissue for CNTs of varying types and concentrations up to 0.1 mg/ml.

4 Discussion

Three different types of CNTs were utilized in our study to allow comparison of optical properties and permit selection of the most efficient absorbers for photothermal therapy. Although previous studies have measured optical properties including refractive index, absorbance, transmittance, reflectance, and absorption coefficients of CNTs in solution,[8,25–35] this is the first study measuring and comparing the absorption and reduced scattering coefficients of SWNTs, MWNTs, and SWNHs as a function of wavelength and concentration in water and tissue representative phantoms. Because the interfacial contact between CNTs and both liquids and solid phantoms may differ, potentially impacting optical properties, both liquid and solid samples were utilized. However, we have observed similar behavior by both types of samples. The inclusion of all types of CNTs in water and phantoms significantly increased light absorption, with minor increases in light scattering.

4.1 Optical Properties of Carbon Nanotubes in Water

The total attenuation coefficient was measured for three types of CNTs in water. Inclusion of all types of CNTs in water for the concentration range (0.01–0.1 mg/ml) significantly increased the light attenuation. We demonstrated that absorption and total attenuation coefficient were nearly identical, indicating the scattering effect of CNTs to be minor (<8%) over the wavelength range of 300–1300 nm [Figs. 3(e)–3(g)]. In our experiments with liquid samples, we found the absorbance of MWNTs to be approximately four fold higher than SWNTs at a concentration of 0.1 mg/ml and wavelength of 1064 nm [Fig. 3(d)]. Previous

Fig. 8 Absorption coefficients of phantoms containing varying CNT types as a function of CNT concentration at a wavelength of 1064 nm.

literature has predicted that the absorbance of MWNTs should be superior to SWNTs, which coincides with our experimental results.[3,61] The absorption of MWNTs is twofold higher than SWNHs and SWNHs possess approximately twofold higher absorption than SWNTs at the same concentration in water with identical wavelength.

The linear relationship of attenuation coefficient with CNT concentration in water [Fig. 3(h)] satisfies Beer's law,[50] which will enable determination of unknown attenuation or absorption coefficient at concentrations up to 0.1 mg/ml at a wavelength of 1064 nm. The linear relationship of attenuation and absorption coefficients is similar to the absorbance study of Kam et al.,[8] where absorbance of noncovalently functionalized SWNTs in water had a linear relationship with SWNT concentration. However, for MWNTs at a concentration of 0.5 mg/ml or greater, the absorption curve became nonlinear, no longer complying with Beer's law. At and beyond this concentration, the sample sufficiently diminishes light transmission, preventing measurement and prohibiting use of this relation for concentration or absorption coefficient determination.

4.2 *Breast Cancer Phantom with Carbon Nanotubes*

Prior to determining the optical properties of phantoms, we confirmed the accuracy of our technique by comparing the absorption and reduced scattering coefficients of pig skin determined by our method with the well-known results of Beek et al.[54] (Fig. 5). Because tissue is composed of nearly 70% water, its absorption coefficient is similar, but slightly higher than water due to the presence of hemoglobin and protein.[50] The absorption profile of all types of phantoms exhibited relative maxima at 970 and 1200 nm, which are the characteristics of well-known water absorption peaks.[2] However, the light-scattering properties vary significantly for different types of tissue due to variation of collagen fibers and blood vessels.[62,63] Sodium alginate, which formed the basis for the breast tumor phantom structure, is highly transparent with optical properties similar to water. Therefore, in order to mimic breast cancer tissue, we incorporated varying concentrations of highly light-scattering particles, including polystyrene beads and talc perfume powder in the sodium alginate to increase the scattering coefficient to more effectively match the actual breast tumor scattering properties [Fig. 4(c)]. The final composition of the breast tumor phantom utilized 1 mg/ml polystyrene beads (3 μm diam) and 40 mg/ml talc powder in alginate, providing a tissue-representative phantom with absorption and reduced scattering coefficients very close to actual breast cancer tumors[47,50] at wavelengths of 800 and 900 nm, as shown in Fig. 4(e) and Table 1.

Inclusion of CNTs in breast cancer phantoms caused the absorption to increase significantly. Absorption coefficients of MWNTs, SWNHs, and SWNTs in phantoms were increased by 21-fold, 9-fold, and 5-fold compared to phantoms without CNTs, respectively [Figs. 6(c), 6(e), and 6(g)] for an identical concentration of 0.1 mg/ml and wavelength of 1064 nm. For the same concentration and wavelength, the change in reduced scattering coefficient is relatively minor with a 1.2- to 1.3-fold increase compared to phantoms without CNTs [Figure 6(d), 6(f), and 6(h)].

4.3 *Comparison of Multiwalled Carbon Nanotubes, Single-Walled Carbon Nanotubes, and Single-Walled Carbon Nanohorns*

Phantoms containing MWNTs possess the highest absorption coefficient. MWNTs absorb light approximately four times greater than SWNTs and 2 times greater than SWNHs for a CNT concentration of 0.1 mg/ml in phantoms at the wavelength of 1064 nm [Fig. 7(a)]. A similar phenomenon was observed for CNTs in water, where MWNTs possessed approximately four and two times higher absorption than SWNTs and SWNHs, respectively, at a concentration of 0.1 mg/ml [Fig. 3(d)]. Previous literature predicted that MWNTs may possess superior light-absorbing capacity compared to SWNTs,[3,61,64] which was confirmed by our study. CNTs in water and phantoms exhibit similar, but not identical absorption and scattering coefficients, which may be due to the absorption by beads and talc powder in phantoms and difference of interfacial contact for CNTs with solids and liquids.

Variation in scattering effects among different types of CNTs is <1% for an identical concentration confirming inclusion of various types of CNTs has minimal effect on the scattering properties of a media. The measured optical properties of breast cancer representative phantoms with inclusion of CNTs provide an estimate of the effects CNTs may have on the overall optical properties of real tumor tissue. Similar to CNTs in water [Fig. 3(h)], the absorption coefficient of solid breast cancer phantoms containing CNTs increase linearly with rising CNT concentrations (Fig. 8).

5 Conclusion

This is the first study investigating the impact of inclusion of varying CNT type and concentration on the optical properties of tissue representative phantoms. Absorption coefficients increased significantly following introduction of CNTs in solutions and phantoms. Phantoms containing MWNTs possessed the highest absorption coefficients. Changes in scattering coefficient of tissue phantoms were negligible following CNT inclusion, implying CNTs are predominantly light-absorbing materials with negligible scattering. It is anticipated that tumor tissue injected with CNTs will have similar absorption and scattering properties as those determined for tissue-representative sodium alginate phantoms incorporated with CNTs. The optical properties determined in this study will provide valuable input parameters for treatment planning models for predicting and optimizing tissue response to photothermal therapies utilized in combination with CNTs.

References

1. A. Burke, X. F. Ding, R. Singh, R. A. Kraft, N. Levi-Polyachenko, M. N. Rylander, C. Szot, C. Buchanan, J. Whitney, J. Fisher, H. C. Hatcher, R. D'Agostino, N. D. Kock, P. M. Ajayan, D. L. Carroll, S. Akman, F. M. Torti, and S. V. Torti, "Long-term survival following a single treatment of kidney tumors with multiwalled carbon nanotubes and near-infrared radiation," *Proc. Nat. Acad. Sci. U. S. A.* **106**(31), 12897–12902 (2009).

2. S. Sarkar, J. Fisher, C. Rylander, and M. N. Rylander, "Photothermal response of tissue phantoms containing multi-walled carbon nanotubes," *J. Biomech. Eng.* **132**(4), 044505 (2010).

3. S. V. Torti, F. Byrne, O. Whelan, N. Levi, B. Ucer, M. Schmid, F. M. Torti, S. Akman, J. Liu, P. M. Ajayan, O. Nalamasu, and D. L. Carroll, "Thermal ablation therapeutics based on CNx multi-walled nanotubes," *Int. J. Nanomed.* **2**(4), 707–714 (2007).

4. Y. Feng, D. Fuentes, A. Hawkins, J. Bass, M. Rylander, A. Elliott, A. Shetty, R. Stafford, and J. Oden, "Nanoshell-mediated laser surgery simulation for prostate cancer treatment," *Eng. Comput.* **25**(1), 3–13 (2009).

5. M. N. Rylander, Y. Feng, J. Bass, and K. R. Diller, "Heat shock protein expression and injury optimization for laser therapy design," *Lasers Surg. Med.* **39**(9), 731–746 (2007).

6. M. N. Rylander, Y. Feng, Y. Zhang, J. Bass, R. J. Stafford, A. Volgin, J. D. Hazle, and K. R. Diller, "Optimizing heat shock protein expression induced by prostate cancer laser therapy through predictive computational models," *J. Biomed. Opt.* **11**(4), 041113 (2006).

7. J. T. Beckham, M. A. Mackanos, C. Crooke, T. Takahashi, C. O'Connell-Rodwell, C. H. Contag, and E. Duco Jansen, "Assessment of cellular response to thermal laser injury through bioluminescence imaging of heat shock protein 70," *Photochem. Photobiol.* **79**(1), 76–85 (2004).

8. N. W. S. Kam, M. O'Connell, J. A. Wisdom, and H. J. Dai, "Carbon nanotubes as multifunctional biological transporters and near-infrared agents for selective cancer cell destruction," *Proc. Nat. Acad. Sci. U. S. A.* **102**(33), 11600–11605 (2005).

9. A. Bassil, P. Puech, L. Tubery, W. Bacsa, and E. Flahaut, "Controlled laser heating of carbon nanotubes," *Appl. Phys. Lett.* **88**(17), 173113 (2006).

10. M. S. Dresselhaus, G. Dresselhaus, and P. C. Eklund, *Science of Fullerenes and Carbon Nanotubes*, Academic Press, New York (1996).

11. E. Miyako, H. Nagata, K. Hirano, K. Sakamoto, Y. Makita, K. Nakayama, and T. Hirotsu, "Photoinduced antiviral carbon nanohorns," *Nanotechnology* **19**(7), 475103 (2008).

12. J. Miyawaki, M. Yudasaka, T. Azami, Y. Kubo, and S. Iijima, "Toxicity of single-walled carbon nanohorns," *Acs Nano* **2**(2), 213–226 (2008).

13. N. B. Saleh, L. D. Pfefferle, and M. Elimelech, "Aggregation kinetics of multiwalled carbon nanotubes in aquatic systems: measurements and environmental implications," *Env. Sci. Technol.* **42**(21), 7963–7969 (2008).

14. N. B. Saleh, L. D. Pfefferle, and M. Elimelech, "Influence of biomacro-molecules and humic acid on the aggregation kinetics of single-walled carbon nanotubes," *Env. Sci. Technol.* **44**(7), 2412–2418 (2010).

15. X. Fan, J. Tan, G. Zhang, and F. Zhang, "Isolation of carbon nanohorn assemblies and their potential for intracellular delivery," *Nanotechnology* **18**(19), 195103 (2007).

16. S. Iijima, M. Yudasaka, R. Yamada, S. Bandow, K. Suenaga, F. Kokai, and K. Takahashi, "Nano-aggregates of single-walled graphitic carbon nano-horns," *Chem. Phys. Lett.* **309**(3–4), 165–170 (1999).

17. X. Sun, R. Q. Yu, G. Q. Xu, T. S. A. Hor, and W. Ji, "Broadband optical limiting with multiwalled carbon nanotubes," *Appl. Phys. Lett.* **73**(25), 3632–3634 (1998).

18. R. R. Anderson and J. A. Parrish, "The optics of human-skin," *J. Invest. Dermatol.* **77**(1), 13–19 (1981).

19. P. J. Burke, S. D. Li, and Z. Yu, "Quantitative theory of nanowire and nanotube antenna performance," *IEEE Trans. Nanotechnol.* **5**(4), 314–334 (2006).

20. G. W. Hanson, "Fundamental transmitting properties of carbon nanotube antennas," *IEEE Trans. Antennas Propagat.* **53**(11), 3426–3435 (2005).

21. K. Kempa, J. Rybczynski, Z. P. Huang, K. Gregorczyk, A. Vidan, B. Kimball, J. Carlson, G. Benham, Y. Wang, A. Herczynski, and Z. F. Ren, "Carbon nanotubes as optical antennae," *Adv. Mater.* **19**(3), 421–426 (2007).

22. Y. Wang, K. Kempa, B. Kimball, J. B. Carlson, G. Benham, W. Z. Li, T. Kempa, J. Rybczynski, A. Herczynski, and Z. F. Ren, "Receiving and transmitting light-like radio waves: Antenna effect in arrays of aligned carbon nanotubes," *Appl. Phys. Lett.* **85**(13), 2607–2609 (2004).

23. J. W. Fisher, S. Sarkar, C. F. Buchanan, C. S. Szot, J. Whitney, H. C. Hatcher, S. V. Torti, C. G. Rylander, and M. N. Rylander, "Photothermal response of human and murine cancer cells to multiwalled carbon nanotubes and laser irradiation," *Cancer Res.* **70**(23), 9855–9864 (2010).

24. J. R. Whitney, S. Sarkar, J. Zhang, T. Do, T. Young, M. K. Manson, T. A. Campbell, A. A. Puretzky, C. M. Rouleau, K. L. More, D. B. Geohegan, C. G. Rylander, H. C. Dorn, and M. N. Rylander, "Single walled carbon nanohorns as photothermal cancer agents," *Lasers Surg. Med.* **43**(1), 43–51 (2011).

25. C. Saltiel, S. Manickavasagam, M. P. Menguc, and R. Andrews, "Light-scattering and dispersion behavior of multiwalled carbon nanotubes," *J. Opt. Soc. Am. A* **22**(8), 1546–1554 (2005).

26. E. Malic, M. Hirtschulz, F. Milde, Y. Wu, J. Maultzsch, T. F. Heinz, A. Knorr, and S. Reich, "Theory of Rayleigh scattering from metallic carbon nanotubes," *Phys. Rev. B* **77**(4), 045432 (2008).

27. A. G. Rozhin, Y. Sakakibara, M. Tokumoto, H. Kataura, and Y. Achiba, "Near-infrared nonlinear optical properties of single-wall carbon nan-otubes embedded in polymer film," *Thin Solid Films* **464–465**, 368–372 (2004).

28. A. Casey, G. F. Farrell, M. McNamara, H. J. Byrne, and G. Chambers, "Interaction of carbon nanotubes with sugar complexes," *Synth. Met.* **153**(1–3), 357–360 (2005).

29. V. Scardaci, Z. P. Sun, F. Wang, A. G. Rozhin, T. Hasan, F. Hennrich, I. H. White, W. I. Milne, and A. C. Ferrari, "Carbon nanotube polycarbonate composites for ultrafast lasers," *Adv. Mater.* **20**(21), 4040–4043 (2008).

30. S. M. O'Flaherty, S. V. Hold, M. E. Brennan, M. Cadek, A. Drury, J. N. Coleman, and W. J. Blau, "Nonlinear optical response of multiwalled carbon-nanotube dispersions," *J. Opt. Soc. Am. B* **20**(1), 49–58 (2003).

31. M. Husanu, M. Baibarac, and I. Baltog, "Particular signature of isolated and bundled carbon nanotubes in their Raman spectra," *Romanian Rep. Phys.* **60**(3), 691–699 (2008).

32. Z. Guo, F. Du, D. M. Ren, Y. S. Chen, J. Y. Zheng, Z. B. Liu, and J. G. Tian, "Covalently porphyrin-functionalized single-walled carbon nan-otubes: a novel photoactive and optical limiting donor-acceptor nanohybrid," *J. Mater. Chem.* **16**(29), 3021–3030 (2006).

33. S. H. Jeong, K. K. Kim, S. J. Jeong, K. H. An, S. H. Lee, and Y. H. Lee, "Optical absorption spectroscopy for determining carbon nanotube concentration in solution," *Synth. Met.* **157**(13–15), 570–574 (2007).

34. E. Kymakis and G. A. J. Amaratunga, "Optical properties of polymer-nanotube composites," *Synth. Met.* **142**(1–3), 161–167 (2004).

35. D. V. Khudyakov, A. S. Lobach, and V. A. Nadtochenko, "Nonlinear optical absorption of single-wall carbon nanotubes in carboxymethyl-cellulose thin polymer film and its application as a saturable absorber for mode-locking in pulsed Nd:glass laser," *Appl. Opt.* **48**(8), 1624–1627 (2009).

36. E. M. Patterson, C. E. Shelden, and B. H. Stockton, "Kubelka-munk optical-properties of a barium-sulfate white reflectance standard," *Appl. Opt.* **16**(3), 729–732 (1977).

37. H. J. Wei, D. Xing, G. Y. Wu, H. M. Gu, F. J. Lu, Y. Jin, and X. Y. Li, "Differences in optical properties between healthy and pathological human colon tissues using a Ti:sapphire laser: an *in vitro* study using the Monte Carlo inversion technique," *J. Biomed. Opt.* **10**(4), 044022 (2005).

38. M. Firbank, M. Hiraoka, M. Essenpreis, and D. T. Delpy, "Measurement of the optical-properties of the skull in the wavelength range 650–950 nm," *Phys. Med. Biol.* **38**(4), 503–510 (1993).

39. T. L. Troy and S. N. Thennadil, "Optical properties of human skin in the near infrared wavelength range of 1000 to 2200 nm," *J. Biomed. Opt.* **6**(2), 167–176 (2001).

40. S. A. Prahl, M. J. C. Vangemert, and A. J. Welch, "Determining the optical-properties of turbid media by using the adding-doubling method," *Appl. Opt.* **32**(4), 559–568 (1993).

41. D. D. Royston, R. S. Poston, and S. A. Prahl, "Optical properties of scattering and absorbing materials used in the development of optical phantoms at 1064 nm," *J. Biomed. Opt.* **1**(1), 110–116 (1996).

42. N. Honda, K. Ishii, A. Kimura, M. Sakai, and K. Awazu, "Determination of optical property changes by laser treatments using inverse adding-doubling method," *Proc. SPIE* **7175**, 71750Q (2009).

43. M.-D. Cheng, D.-W. Lee, B. Zhao, H. Hu, D. J. Styers-Barnett, A. A. Puretzky, D. W. DePaoli, D. B. Geohegan, E. A. Ford, and P. Angelini, "Formation studies and controlled production of carbon nanohorns using continuous in situ characterization techniques," *Nanotechnology* **18**(18), 185604 (2007).

44. D. Geohegan, A. Puretzky, I. Ivanov, G. Eres, Z. Liu, D. Styers-Barnett, H. U. I. Hu, B. I. N. Zhao, H. Cui, C. Rouleau, S. Jesse, P. Britt, H. Christen, K. A. I. Xiao, P. Fleming, and A. L. Meldrum, "Laser-based synthesis, diagnostics, and control of single-walled carbon nanotubes and nanohorns for composites and biological nanovectors," *Photon-based Nanoscience and Nanobiotechnology* **239**, 205–223 (2006).

45. S. Sarkar and M. N. Rylander, "Measurement of thermal conductivity of carbon nanotube-tissue phantom composites with hot wire probe method," *Ann. Biomed. Eng.* (in press).

46. M. Lualdi, A. Colombo, B. Farina, S. Tomatis, and R. Marchesini, "A phantom with tissue-like optical properties in the visible and near infrared for use in photomedicine," *Lasers Surg. Med.* **28**(3), 237–243 (2001).

47. J. C. Hebden, D. J. Hall, M. Firbank, and D. T. Delpy, "Time-resolved optical imaging of a solid tissue-equivalent phantom," *Appl. Opt.* **34**(34), 8038–8047 (1995).

48. C. S. D. Lee, J. P. Gleghorn, N. Won Choi, M. Cabodi, A. D. Stroock, and L. J. Bonassar, "Integration of layered chondrocyte-seeded alginate hydrogel scaffolds," *Biomaterials* **28**(19), 2987–2993 (2007).

49. M. Wong, "Alginates in tissue engineering," in *Biopolymer Methods in Tissue Engineering*, pp. 77–86, Humana Press, Totowa, NJ (2003).

50. A. J. Welch and M. Gemert, *Optical-Thermal Response of Laser Irradiated Tissue*, Plenum Press, New York (1995).

51. L. V. Wang and H. Wu, *Biomedical Optics Principles and Imaging*, Wiley, Hoboken, NJ (2007).

52. J. Kim, D. P. Davé, C. G. Rylander, J. Oh, and T. E. Milner, "Spatial refractive index measurement of porcine artery using differential phase optical coherence microscopy," *Lasers Surg. Med.* **38**(10), 955–959 (2006).

53. W. V. Sorin and D. F. Gray DF, "Simultaneous thickness and group index measurement using optical low-coherence reflectometry," *IEEE Photonics Technology Lett.* **4**(1), 105–107 (1992).

54. J. F. Beek, P. Blokland, P. Posthumus, M. Aalders, J. W. Pickering, H. J. C. M. Sterenborg, and M. J. C. V. Gemert, "*In vitro* double-integrating-sphere optical properties of tissues between 630 and 1064 nm," *Phys. Med. Biol.* **42**(11), 2255 (1997).

55. G. M. Hale and M. R. Query, "Optical constants of water in the 200-nm to 200-μm wavelength region," *Appl. Opt.* **12**(3), 555–563 (1973).

56. H. Key, E. R. Davies, P. C. Jackson, and P. N. T. Wells, "Optical attenuation characteristics of breast tissues at visible and near-infrared wavelengths," *Phys. Med. Biol.* **36**(5), 579 (1991).

57. V. G. Peters, D. R. Wyman, M. S. Patterson, and G. L. Frank, "Optical properties of normal and diseased human breast tissues in the visible and near infrared," *Phys. Med. Biol.* **35**(9), 1317 (1990).

58. Ó. Esteban, F. Marvá, and J. C. Martínez-Antón, "Optical constants of a sodium alginate polymer in the UV-vis range," *Opt. Mater.* **31**(4), 696–699 (2009).

59. I. Niskanen, J. Raty, and K. E. Peiponen, "Estimation of effective refractive index of birefringent particles using a combination of the immersion liquid method and light scattering," *Appl. Spectrosc.* **62**(4), 399–401 (2008).

60. B. Gates, S. H. Park, and Y. N. Xia, "Tuning the photonic bandgap properties of crystalline arrays of polystyrene beads by annealing at elevated temperatures," *Adv. Mater.* **12**(9), 653–656 (2000).

61. N. Levi-Polyachenko, D. L. Carroll, and J. H. Stewart, *Applications of Carbon-Based Nanomaterials for Drug Delivery in Oncology*, Springer, Netherlands (2008).

62. K. Vishwanath, D. Klein, K. Chang, T. Schroeder, M. W. Dewhirst, and N. Ramanujam, "Quantitative optical spectroscopy can identify long-term local tumor control in irradiated murine head and neck xenografts," *J. Biomed. Opt.* **14**(5), 054051 (2009).

63. J. Q. Brown, L. G. Wilke, J. Geradts, S. A. Kennedy, G. M. Palmer, and N. Ramanujam, "Quantitative Optical spectroscopy: a robust tool for direct measurement of breast cancer vascular oxygenation and total hemoglobin content *in vivo*," *Cancer Res.* **69**(7), 2919–2926 (2009).

64. M. E. Brennan, J. N. Coleman, A. Drury, B. Lahr, T. Kobayashi, and W. J. Blau, "Nonlinear photoluminescence from van Hove singularities in multiwalled carbon nanotubes," *Opt. Lett.* **28**(4), 266–268 (2003).